Catalysts **2015**, *5*, 1554-1573; doi:10.3390/catal5031554

OPEN ACCESS

catalysts

ISSN 2073-4344

www.mdpi.com/journal/catalysts

Article

Bismuth Molybdate Catalysts Prepared by Mild Hydrothermal Synthesis: Influence of pH on the Selective Oxidation of Propylene

Kirsten Schuh [1], Wolfgang Kleist [1,2], Martin Høj [3], Vanessa Trouillet [4], Pablo Beato [5], Anker Degn Jensen [3] and Jan-Dierk Grunwaldt [1,2,*]

1 Institute for Chemical Technology and Polymer Chemistry (ITCP), Karlsruhe Institute of Technology (KIT), Engesserstr. 20, 76131 Karlsruhe, Germany;
E-Mails: kirsten.schuh@gmx.de (K.S.); wolfgang.kleist@kit.edu (W.K.)

2 Institute of Catalysis Research and Technology (IKFT), Karlsruhe Institute of Technology (KIT), Hermann-von-Helmholtz-Platz 1, 76344 Eggenstein-Leopoldshafen, Germany

3 Department of Chemical & Biochemical Engineering, Technical University of Denmark (DTU), Søltofts Plads Building 229, DK-2800 Kgs. Lyngby, Denmark;
E-Mails: mh@kt.dtu.dk (M.H.); aj@kt.dtu.dk (A.D.J.)

4 Institute for Applied Materials (IAM) and Karlsruhe Nano Micro Facility (KNMF), Karlsruhe Institute of Technology (KIT), Hermann-von-Helmholtz-Platz 1, 76344 Eggenstein-Leopoldshafen, Germany; E-Mail: vanessa.trouillet@kit.edu

5 Haldor Topsøe A/S, Nymøllevej 55, DK-2800 Kgs. Lyngby, Denmark; E-Mail: pabb@topsoe.dk

* Author to whom correspondence should be addressed; E-Mail: grunwaldt@kit.edu;
Tel.: +49-721-608-42120; Fax: +49-721-608-44820.

Academic Editor: Keith Hohn

Received: 20 July 2015 / Accepted: 25 August 2015 / Published: 10 September 2015

Abstract: A series of bismuth molybdate catalysts with relatively high surface area was prepared via mild hydrothermal synthesis. Variation of the pH value and Bi/Mo ratio during the synthesis allowed tuning of the crystalline Bi-Mo oxide phases, as determined by X-ray diffraction (XRD) and Raman spectroscopy. The pH value during synthesis had a strong influence on the catalytic performance. Synthesis using a Bi/Mo ratio of 1/1 at pH ≥ 6 resulted in γ-Bi_2MoO_6, which exhibited a better catalytic performance than phase mixtures obtained at lower pH values. However, a significantly lower catalytic activity was observed at pH = 9 due to the low specific surface area. γ-Bi_2MoO_6 synthesized with Bi/Mo = 1/1 at pH = 6 and 7 exhibited relatively high surface areas and the best catalytic performance. All

samples prepared with Bi/Mo = 1/1, except samples synthesized at pH = 1 and 9, showed better catalytic performance than samples synthesized with Bi/Mo = 2/3 at pH = 4 and 9 and γ-Bi_2MoO_6 synthesized by co-precipitation at pH = 7. At temperatures above 440 °C, the catalytic activity of the hydrothermally synthesized bismuth molybdates started to decrease due to sintering and loss of surface area. These results support that a combination of the required bismuth molybdate phase and a high specific surface area is crucial for a good performance in the selective oxidation of propylene.

Keywords: hydrothermal synthesis; bismuth molybdate; effect of pH; propylene oxidation; acrolein

1. Introduction

Since the development of bismuth molybdate catalysts for the oxidation and ammoxidation of propylene to acrolein or acrylonitrile by Sohio in 1959 [1,2], these mixed oxides have received strong attention and their catalytic properties have been studied in considerable detail [3–12]. Addition of further elements such as iron, cobalt or vanadium increased the acrolein and acrylonitrile yields and stabilized the catalyst during the reaction. Nevertheless, the surface layer of these multicomponent catalysts consists of mixed oxides based on Bi and Mo, and these two metals seem to form the key active sites [13]. The rate-determining step is the abstraction of hydrogen from propylene on bismuth or bismuth connected to molybdyl groups [14]. The addition of other transition metals and main group metals helps to increase the specific surface area of the catalyst [15], the extent of lattice oxygen participation [15,16] and the electronic conductivity [17]. α-$Bi_2Mo_3O_{12}$, β-$Bi_2Mo_2O_9$ and γ-Bi_2MoO_6 are the bismuth molybdate phases of significance for the selective oxidation of propylene to acrolein. Despite of intensive research there is still a debate in literature about the relative activity of these bismuth molybdate phases and the influence of the preparation route. Thus, the search for new synthesis approaches remains a key issue.

Carson *et al.* [18] stated that the catalytic activity for propylene oxidation decreases in the following order: α > γ > β. On the other hand, γ-Bi_2MoO_6 was found to be the most active phase by Krenzke *et al.* [19] and Monnier *et al.* [20]. Brazdil *et al.* [21] even reported β-$Bi_2Mo_2O_9$ to be more active than the other two bismuth molybdate phases. We recently used flame spray pyrolysis for synthesis [22] and observed that the catalytic activity decreased in the following order: β > γ > α. Furthermore, Snyder and Hill [23] claimed that the stability of the different bismuth molybdate phases, in particular β-$Bi_2Mo_2O_9$, depended on the temperature at which they were calcined.

The most common method to prepare bismuth molybdate catalysts is co-precipitation [9,10,18,19,24–26], but also solid-state routes [27], sol-gel synthesis [28], and spray drying of aqueous solutions [11,29] have been used. All of these methods require heating or calcination at temperatures >400 °C to yield crystalline materials, which may result in a decrease of the catalytic performance of the resulting phase due to bismuth enrichment of the catalyst surface [30]. Recently, γ-Bi_2MoO_6 with relatively high surface area (14 m^2/g) and good catalytic performance was reported using mesoporous carbon templates [31].

Alternatively, bismuth molybdates can be prepared by hydrothermal synthesis [32–38], which is a typical soft chemistry ("chimie douce") method and provides convenient access to advanced materials of high purity, controlled morphology, high crystallinity and good reproducibility [39]. α-$Bi_2Mo_3O_{12}$ (monoclinic, defective fluorite structure) and γ-Bi_2MoO_6 (orthorhombic, layered Aurivillius-type structure) have been successfully synthesized by a one-step synthesis under hydrothermal conditions applying different precursors and various synthesis conditions [32,33,36,40,41]. For the preparation of metastable, monoclinic β-$Bi_2Mo_2O_9$ the precursors were applied in the ratio Bi/Mo = 1/1 leading to a phase mixture which had to be further calcined at 560 °C to obtain crystalline β-bismuth molybdate [33,36]. The crystal growth and the formation of the various bismuth molybdate phases under hydrothermal conditions was studied *in situ* by time-resolved energy dispersive X-ray diffraction (EDXRD) and X-ray absorption spectroscopy (XAS) [33] and by combined EDXRD/XAS/Raman techniques [38]. Kongmark *et al.* [38] reported that $[MoO_4]^{2-}$ entities are required for the formation of γ-Bi_2MoO_6, demonstrating the importance of the pH value in the initial solution for the formation of the desired phase. Li *et al.* [36] successfully synthesized α- and γ-bismuth molybdate from bismuth nitrate and ammonium heptamolybdate with relatively high specific surface area (38–57 m^2/g) compared to other unsupported bismuth molybdate catalysts (1–4 m^2/g) [9,10,29,42] by variation of the pH between 1 and 9. Hydrothermally synthesized bismuth molybdates were mostly applied in photocatalysis under visible light irradiation [36,40,43], where, especially, γ-Bi_2MoO_6 is attractive due to its layered structure.

Although the controlled preparation of unsupported bismuth molybdate catalysts exposing a high surface area under mild conditions seems very attractive for the selective oxidation of olefins, hydrothermally prepared ones have hardly been applied in oxidation reactions. Hydrothermal synthesis as a preparation route for selective oxidation catalysts has been reported for example for iron molybdates [44], $La_{2-x}Sr_xCuO_4$ [45], wolframite type $MMoWO_x$ (with M = Ni and Co) [46] and more complex mixed oxides based on molybdenum and vanadium [47–49]. We have recently shown that hydrothermally synthesized bismuth molybdates were active catalysts for the oxidation of propylene to acrolein [50] and found that the use of nitric acid led to an improved catalytic performance. To further explore catalysts with higher surface area and altered structure, we have systematically studied the performance of hydrothermally synthesized bismuth molybdates. They were prepared under mild hydrothermal conditions by variation of the pH value, which should alter the structure of bismuth molybdates as reported by Li *et al.* [36] To understand the role of the composition and the surface area on the catalytic activity, the resulting product phases, the ratio of bismuth to molybdenum in the bulk and on the surface, as well as the specific surface area have been characterized and correlated to the performance in the selective oxidation of propylene to acrolein. This knowledge may in the future be applied to more complex systems, such as multicomponent molybdenum oxides.

2. Results and Discussion

2.1. Characterization of the Samples Synthesized with Bi/Mo = 1/1

The X-ray diffraction (XRD) patterns and Raman spectra of the samples synthesized with Bi/Mo = 1/1 revealed a strong influence of the pH value on the structure under hydrothermal conditions (Figure 1). At high pH values (pH ≥ 6) γ-Bi_2MoO_6 was formed, which is indicated by the reflections at

2θ = 28.3°, 32.6°, 33.1°, 36.1°, 46.7°, 47.2° in the XRD patterns (Figure 1a; JCPDS card No. 77-1246). The corresponding Raman spectra showed bands at 848 cm^{-1} and 807 cm^{-1} as well as at 719 cm^{-1}, which were ascribed to γ-Bi_2MoO_6 [36,51]. Analysis of the bismuth and molybdenum concentration of the products by ICP-OES led to a Bi/Mo bulk ratio of 1.8–2.1 for pH = 6–9 (Table 1) suggesting that molybdenum partly remained in solution in the form of MoO_4^{2-} [38,52], which was washed away during filtration, and, thus, did not precipitate at high pH values.

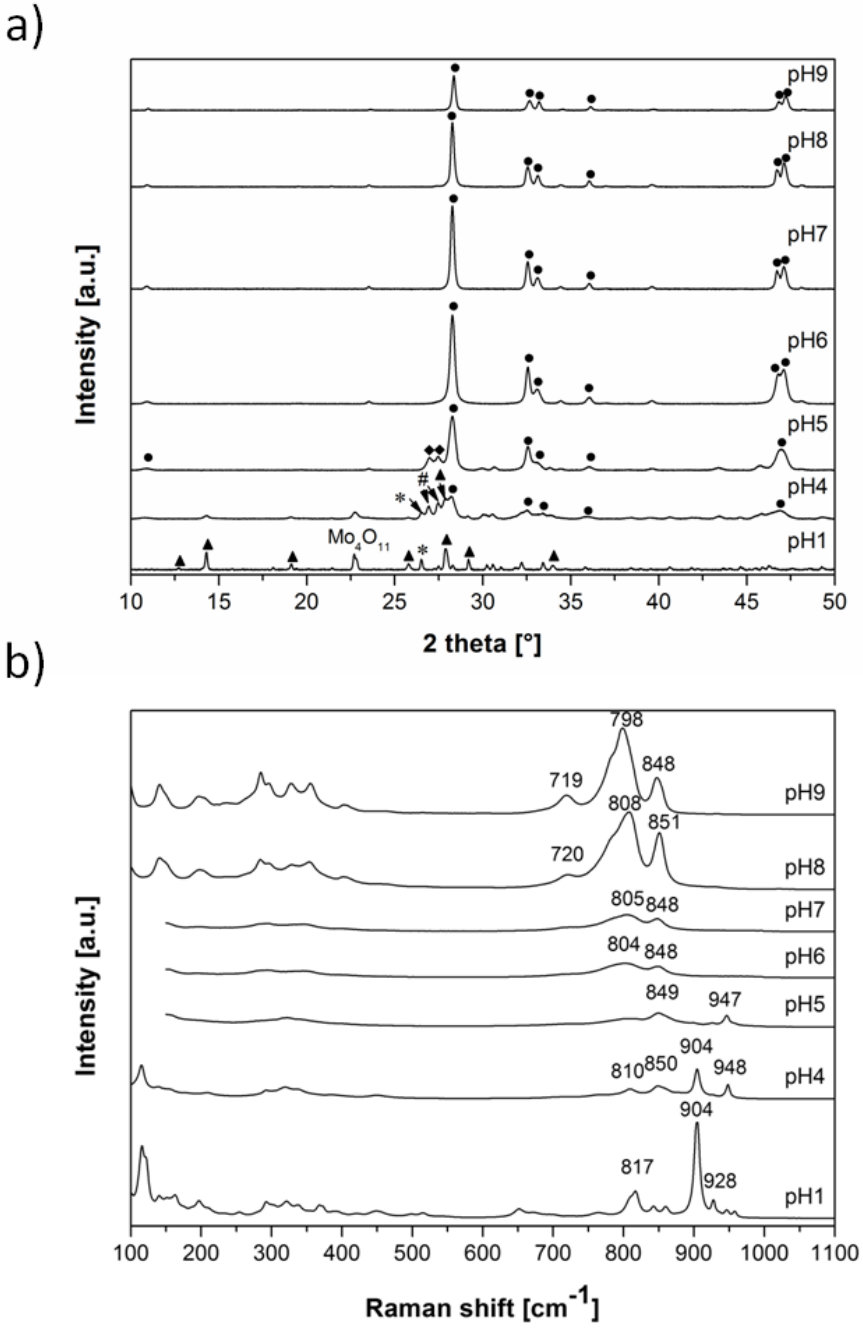

Figure 1. XRD patterns (**a**) and Raman spectra (**b**) of the samples with Bi/Mo = 1/1 at different pH values. The following symbols are used for the different phases: α-$Bi_2Mo_3O_{12}$ (▲), γ-Bi_2MoO_6 (●), $MoO_3 \cdot 2H_2O$ (♦), Bi_2O_3 (*) and $Bi_{26}Mo_{10}O_{69}$ (#).

Table 1. Characterization of the samples prepared by hydrothermal synthesis with different Bi/Mo ratios and at various pH values by X-ray diffraction measurements and Raman spectroscopy, as well as nitrogen physisorption measurements (BET), ICP-OES and XPS (main phases in bold letters).

Sample	Phases According to XRD	Phases According to Raman	Surface Area (BET) [m^2/g]	Bi/Mo Ratio Bulk [a]	Bi/Mo Ratio Surface [b]
		Initial ratio Bi/Mo = 2/1			
Bi2Mo1_pH7	γ-Bi_2MoO_6	-	13	-	-
Bi2Mo1_pH8	γ-Bi_2MoO_6	-	7	-	-
		Initial ratio Bi/Mo = 1/1			
Bi1Mo1_pH1	**α-$Bi_2Mo_3O_{12}$**, Mo_4O_{11}, Bi_2O_3	α-$Bi_2Mo_3O_{12}$	3	1.0	-
Bi1Mo1_pH4	**γ-Bi_2MoO_6**, **α-$Bi_2Mo_3O_{12}$**, Bi_2O_3, $Bi_{26}Mo_{10}O_{69}$	α-$Bi_2Mo_3O_{12}$, γ-Bi_2MoO_6, β-Bi_2O_3	18	0.9	1.1
Bi1Mo1_pH5	**γ-Bi_2MoO_6**, $MoO_3{\cdot}2H_2O$	γ-Bi_2MoO_6, $Mo_7O_{24}^{6-}$ or $MoO_3(H_2O)_2$	32	1.1	1.1
Bi1Mo1_pH6	γ-Bi_2MoO_6	γ-Bi_2MoO_6	26	1.8	1.7
Bi1Mo1_pH7	γ-Bi_2MoO_6	γ-Bi_2MoO_6	17	1.8	1.8
Bi1Mo1_pH8	γ-Bi_2MoO_6	γ-Bi_2MoO_6	10	1.9	2.5
Bi1Mo1_pH9	γ-Bi_2MoO_6	γ-Bi_2MoO_6	4	2.1	
		Initial ratio Bi/Mo = 2/3			
Bi2Mo3_pH1	**α-$Bi_2Mo_3O_{12}$**, $H_{0.68}(NH_4)_2Mo_{14.16}O_{4.34}{\cdot}6.92H_2O$	α-$Bi_2Mo_3O_{12}$	5	-	-
Bi2Mo3_pH4	**γ-Bi_2MoO_6**, $MoO_3{\cdot}2H_2O$, $Bi_5O_7NO_3$	γ-Bi_2MoO_6, $Mo_7O_{24}^{6-}$ or $MoO_3(H_2O)_2$, NO_3^-	17	-	-
Bi2Mo3_pH9	γ-Bi_2MoO_6	γ-Bi_2MoO_6	5	-	-

[a] The calculated error accounts to around 10%. [b] Average of two XPS measurements at different spots.

In weakly acidic or basic aqueous solutions bismuth nitrate is "hydrolyzed" resulting in the formation of BiO^+ [53]. These bismuthyl subunits react with $(MoO_4)^{2-}$ and precipitate as γ-Bi_2MoO_6 [36,54]. X-ray absorption measurements at the Mo K-edge of the samples synthesized at pH = 6 and pH = 9 confirmed that the products contained only octahedral Mo (γ-Bi_2MoO_6; see Figure S1). In addition to γ-Bi_2MoO_6, a molybdenum oxide phase was formed at pH = 5 indicated by the reflections at 2θ = 26.9° and 27.5°, which could be assigned to $MoO_3{\cdot}2H_2O$ (JCPDS No. 39-363), and by the Raman band at 947 cm^{-1} assigned to the presence of $Mo_7O_{24}^{6-}$. At pH = 3–6 $Mo_7O_{24}^{6-}$ [38,55] and $Mo_2O_7^{2-}$ are the stable polymolybdate species in aqueous solution depending on the temperature [52], which agrees well with the Raman spectra of the solid phase. Bi1Mo1_pH5 exhibited a Bi/Mo bulk ratio of 1.1, which corresponds to the applied ratio and resulted in the largest surface area (32 m^2/g, Table 1) among the different bismuth molybdates. In contrast to Li *et al.* [36], γ-Bi_2MoO_6, and not α-$Bi_2Mo_3O_{12}$, was the most prominent phase as detected by X-ray diffraction (main reflection at 27.9°) or Raman spectroscopy (main band at 904 cm^{-1}) for the sample synthesized at pH = 5. The formation of the α-phase was observed at pH ≤ 4 and minor contributions from other phases were detected in addition to α- and γ-bismuth molybdate. Further decrease of the pH to 1 led to the disappearance of γ-Bi_2MoO_6 in the product and α-$Bi_2Mo_3O_{12}$ was the main phase observed by XRD (Figure 1a). In addition to the reflections at

2θ = 14.1°, 18.1°, 25.9°, 27.9° and 29.2°, which were assigned to α-$Bi_2Mo_3O_{12}$ (JCPDS No. 21-103), two reflections at 22.7° and 26.5° were observed. The reflection at 22.7° could be assigned to Mo_4O_{11} (JCPDS No. 86-1269), but assignment of the reflection at 26.5° was not possible. The corresponding Raman spectra (Figure 1b) showed the characteristic bands of α-$Bi_2Mo_3O_{12}$ (928, 904, 861, 843 and 817 cm^{-1}). For all samples synthesized with a Bi/Mo ratio 1/1, β-$Bi_2Mo_2O_9$ was not detected, neither by X-ray diffraction (27.8°), nor by Raman spectroscopy (884 cm^{-1}), which agrees with literature [33,36] where calcination at 560 °C was required to form the β-phase. The samples synthesized at pH = 1–5 contained bismuth and molybdenum in the ratio 1/1 in the bulk (Table 1), corresponding to the applied ratio in the synthesis.

In addition to the characterization of the phase composition and the resulting Bi/Mo ratio in the bulk, the specific surface area and the Bi/Mo ratio on the surface of the products were determined (see Table 1). The XPS spectra showed one doublet for Bi $4f_{7/2}$ at 159.4 eV and one for Mo $3d_{5/2}$ at 232.7 eV (for representative spectra see Figure S2), which revealed an oxidation state of +3 for bismuth [56] and +6 for molybdenum [57]. The surface composition of the catalysts was calculated using the atom concentrations of both elements, which were determined from the peak area of the spectra. At pH = 4–7, the Bi/Mo ratio on the surface was not the same as the ratio in the bulk (Bi/Mo ≈ 1 for pH = 4 and 5, Bi/Mo ≈ 2 for pH = 6 and 7), whereas at pH = 8 a surface enrichment of bismuth (Bi/Mo = 2.5) was observed by XPS. High Bi/Mo surface ratios were also reported in the literature for γ-Bi_2MoO_6 prepared by different methods (spray drying: 2.4 [29], co-precipitation: 2.6 [10,58]), but the existence of surface Bi_2O_3 could neither be confirmed in literature nor in the present work. The sample synthesized at pH = 5 featured the highest specific surface area (32 m^2/g), whereas with increasing and decreasing pH value the surface area of the resulting product was reduced (Table 1) to 4 m^2/g and 3 m^2/g for pH = 9 and pH = 1, respectively. The product composition did not seem to be a determining factor for the specific surface area, as the two samples with the highest surface area showed different phases resulting in a different Bi/Mo ratio in the bulk and on the surface (Bi/Mo =1.1 for pH = 5 with 32 m^2/g and Bi/Mo =1.8 for pH = 6 with 26 m^2/g).

2.2. Variation of the Bi/Mo Ratio

To elucidate the influence of the applied Bi/Mo ratio on the phases, the amount of molybdenum was increased to Bi/Mo = 2/3. Despite of the higher initial Mo content, even at pH = 9 only γ-Bi_2MoO_6 with a high crystallinity was formed as evidenced by X-ray diffraction (Figure 2a) and Raman spectroscopy (Figure 2b). This indicated that also at low Bi/Mo ratio (*i.e.*, with an excess of molybdenum) bismuth-rich γ-Bi_2MoO_6 was formed at high pH values. The specific surface areas of the two samples synthesized at pH = 9 (Bi1Mo1_pH9 and Bi2Mo3_pH9) were similar (4 m^2/g and 5 m^2/g).

Decreasing the pH to 4 led to the same phase composition as in sample Bi1Mo1_pH4 (γ-Bi_2MoO_6 and $MoO_3 \cdot 2H_2O$), but additionally a nitrate-containing phase was found as indicated by the Raman band at 1047 cm^{-1} (Figure 2b). The reflections in the X-ray diffraction pattern (Figure 2a) at 27.6°, 30.7° and 45.7° could be assigned to $Bi_5O_7NO_3$ (JCPDS No. 51-525). Further decrease of the pH to 1 did not result in the formation of pure α-$Bi_2Mo_3O_{12}$, but an ammonium containing molybdenum oxide phase was additionally formed (see Figure 2 and Table 1).

The applied pH value and, thus, the resulting (poly)molybdate anions in the aqueous solution seem to have a stronger impact on the resulting phase than the applied Bi/Mo ratio. For all three samples synthesized with Bi/Mo = 2/3 the surface area determined by nitrogen physisorption was almost identical to the samples synthesized with Bi/Mo = 1/1 at the same pH value (Table 1).

Using an excess of bismuth and applying the initial ratio Bi/Mo = 2/1 at pH = 7 and pH = 8 led to the formation of highly crystalline γ-Bi_2MoO_6 (see XRD patterns in Figure S3). This is in agreement with Li *et al.* [36] and Zhang *et al.* [40], who also reported that hydrothermal synthesis with Bi/Mo = 2/1 always resulted in γ-Bi_2MoO_6 independent of the pH value (pH = 1–13).

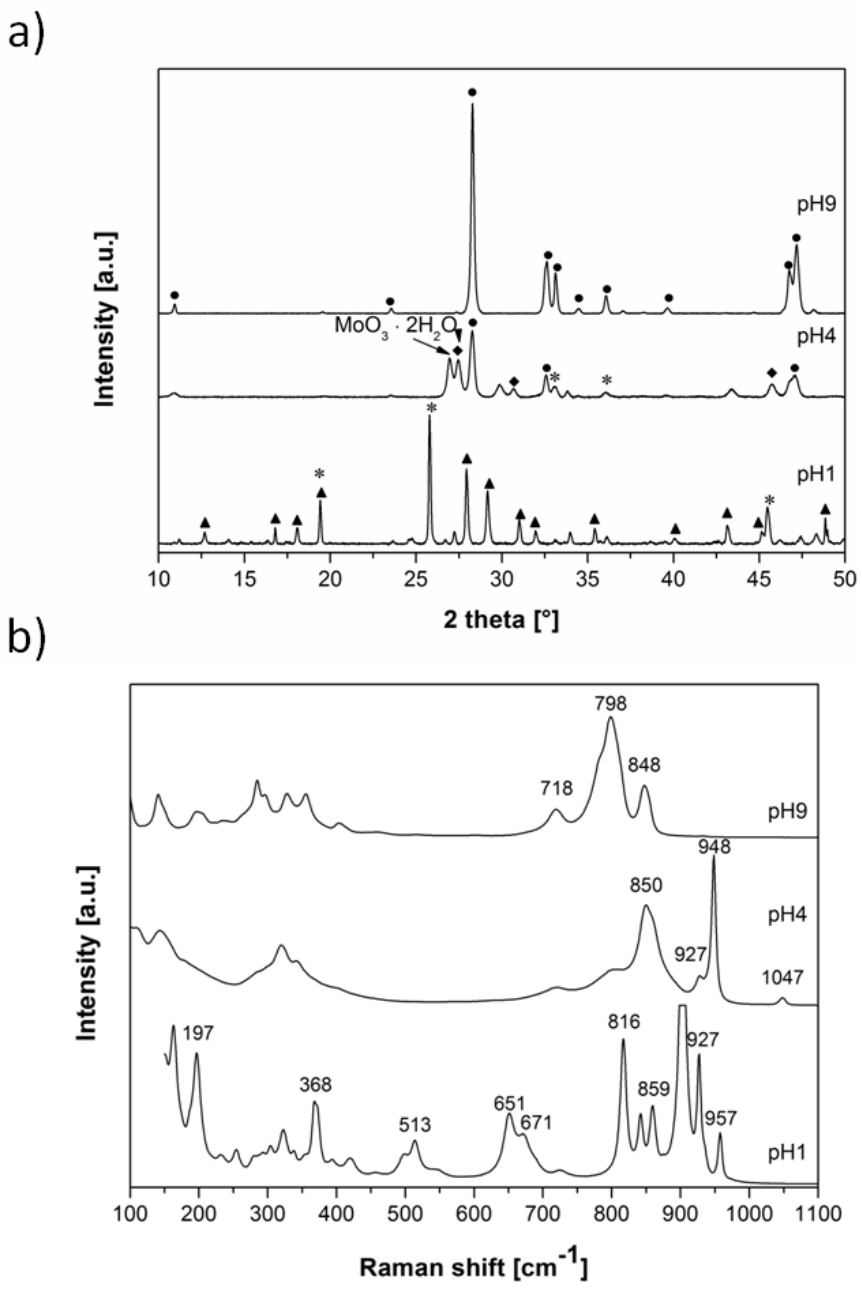

Figure 2. XRD patterns (**a**) and Raman spectra (**b**) of the samples with Bi/Mo = 2/3 at different pH values. The following symbols are used for the different phases: α-$Bi_2Mo_3O_{12}$ (▲), γ-Bi_2MoO_6 (●), $H_{0.68}(NH_4)_2Mo_{14.16}O_{4.34}{\cdot}6.92H_2O$ (*) and $Bi_5O_7NO_3$ (♦).

2.3. Catalytic Performance in Propylene Oxidation to Acrolein

The samples synthesized with Bi/Mo = 1/1 were tested in propylene oxidation at 320 °C–520 °C to study the influence of the preparation parameters, *i.e.*, the pH value and the corresponding structural properties on the catalytic performance of the hydrothermally synthesized bismuth molybdates. Figure 3 depicts the acrolein selectivity as a function of the propylene conversion at different flows (50, 80 and 120 NmL/min) leading to different catalyst contact times and, therefore, to a different propylene conversion and/or acrolein selectivity. At 320 °C (Figure 3a), the sample synthesized at pH = 6 showed the highest propylene conversion (19% and 31% propylene conversion, 74% and 73% acrolein selectivity for 120 NmL/min and 50 NmL/min, respectively), followed by the samples synthesized at pH = 7 ($X_{propylene}$ = 27% and $S_{acrolein}$ = 67% for 50 NmL/min) and pH = 8 ($X_{propylene}$ = 25% and $S_{acrolein}$ = 59% for 50 NmL/min).

Although the surface area of the sample synthesized at pH = 5 was higher, it converted less propylene ($X_{propylene}$ = 10%–21%). Both the samples prepared at pH = 5 and also at pH = 4, which performed even worse (8%–16% conversion of propylene), contained minor amounts of other phases additionally to γ-Bi_2MoO_6. This indicates that the samples which contained only γ-Bi_2MoO_6 were more active than the other samples. However, the sample synthesized at pH = 9, which also only contained crystalline γ-Bi_2MoO_6 but with lower specific surface area, reached propylene conversions of only 2%–4% at acrolein selectivities of 69%–49%. The sample synthesized at pH = 1, exhibiting a small surface area (3 m^2/g), was also nearly inactive, since the propylene conversion remained around 3% for 120–50 NmL/min total flow, while the acrolein selectivity strongly decreased from 80% to 38% with increasing flow.

The major by-products were CO_2 (selectivities around 10%–20%), acetaldehyde (7%–8%) and CO (1%–5%). Ethylene and hexadiene were only detected in very small amounts for the sample Bi1Mo1_pH9 at temperatures above 440 °C.

At 360 °C, the differences in activity between the various samples were less pronounced, but the samples synthesized at pH = 6 and pH = 7 still showed the best catalytic performance (propylene conversion of 40%–56% and 37%–54%, respectively) followed by the sample at pH = 8, which was slightly less selective (acrolein selectivity of 72%–80% compared to 78%–84%; see Figure 3b). All the samples featured significantly higher surface areas than in a previous study, where (i) the precursors were only dissolved in water; (ii) the precursor solutions were not prepared separately; and (iii) the pH was not adjusted by addition of acid or ammonia [50]. In line with previous studies, the use of nitric acid was beneficial and adjusting the pH by ammonia seemed to lead to a rather high surface area.

In Figure 4 the propylene conversion as well as the acrolein yield at 360 °C was correlated to the pH values during hydrothermal synthesis. Propylene conversion and acrolein yield showed volcano-like curves with respect to pH with a maximum at pH = 6. Interestingly, there was a steep increase in conversion from pH = 5 to pH = 6, although the specific surface area was higher at pH = 5. In addition, the samples at pH = 6 and pH = 7 featured a significantly higher Bi/Mo ratio of approximately 2 compared to the sample prepared at pH = 5, both in the bulk and on the surface (Table 1). Comparison of Table 1 and Figure 4 evidenced that a combination of the right bismuth molybdate phase (γ-Bi_2MoO_6) and a high surface area seemed to be important for high propylene conversion. It has been shown that oxygen diffusion through the lattice is most effective for γ-Bi_2MoO_6 compared to the other bismuth

molybdate phases [59]. Thus, it may be rewarding in the future to also correlate the catalytic activity in relation to the nature of lattice oxygen.

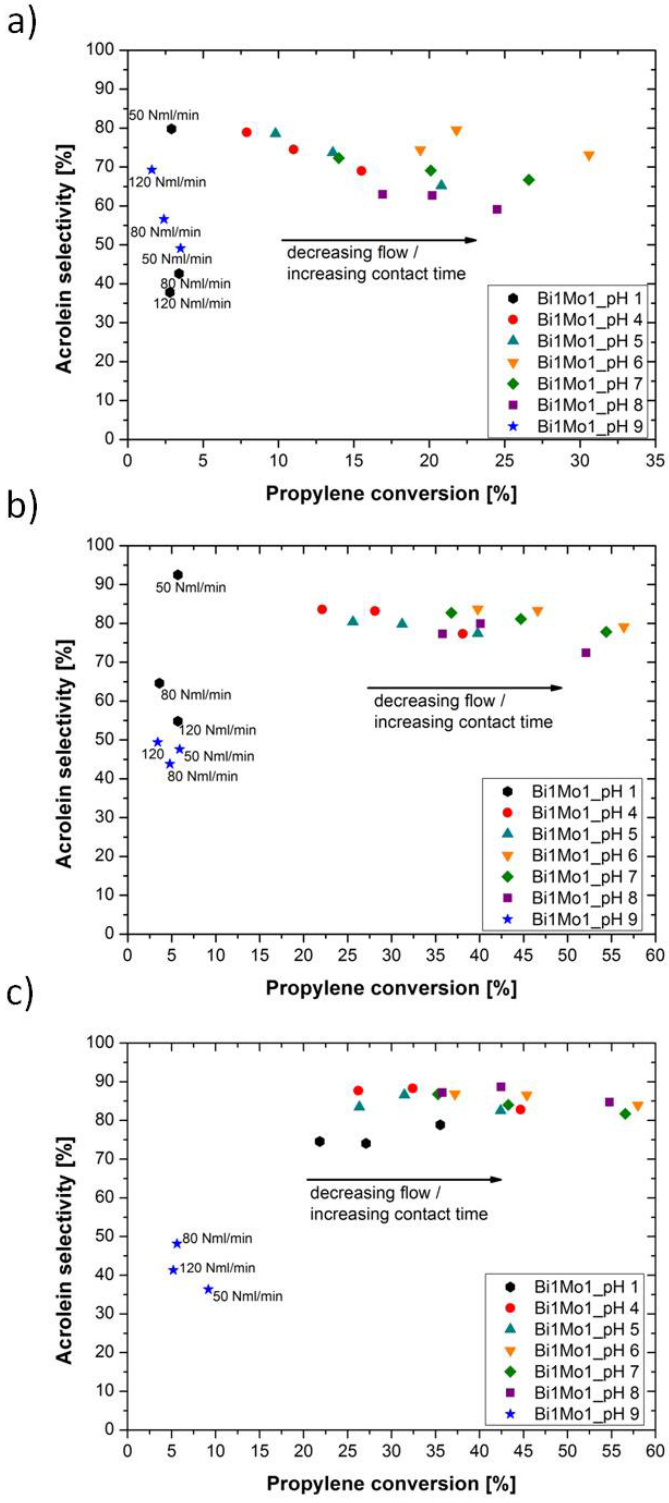

Figure 3. Catalytic performance of samples prepared with Bi/Mo = 1/1 at 320 °C (**a**); 360 °C (**b**) and 400 °C (**c**). The samples were dried in air at room temperature, crushed, sieved and pre-treated in the reactor in synthetic air at 300 °C. Reaction conditions: 500 mg catalyst; $C_3H_6/O_2/N_2$ = 5/25/70; 50, 80 and 120 NmL/min.

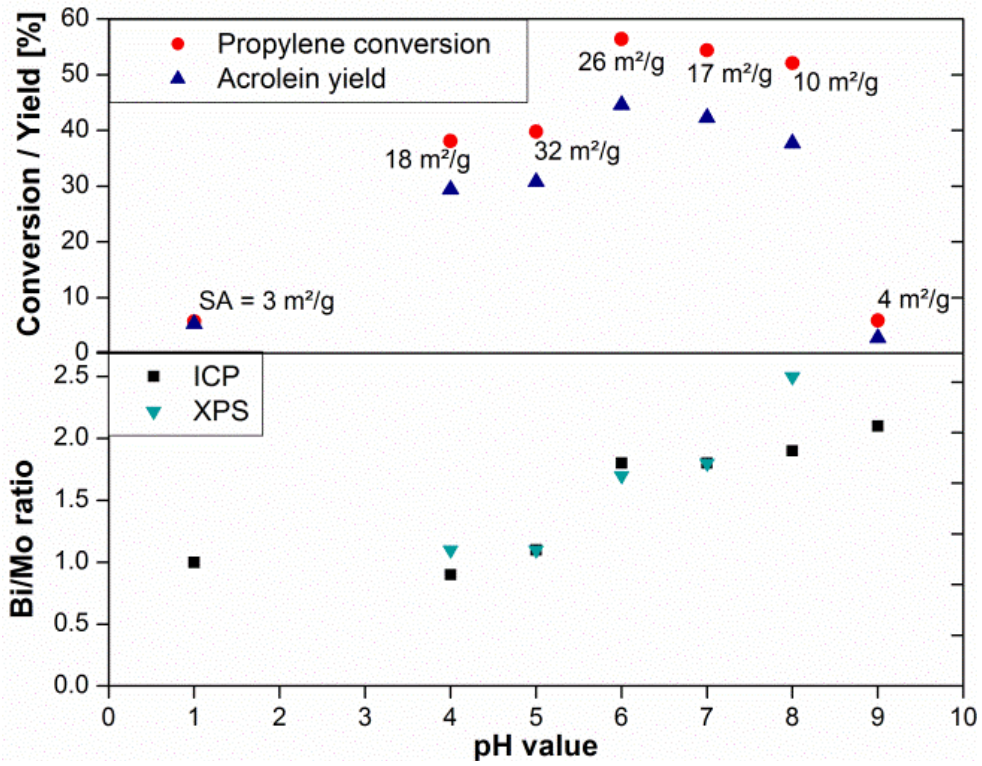

Figure 4. Correlation of the pH value in the initial solution, the Bi/Mo ratio determined in the bulk (ICP) and on the surface (XPS), and the catalytic performance at 360 °C using a flow of 50 NmL/min with a composition of $C_3H_6/O_2/N_2$ = 5/25/70 and 500 mg of catalyst.

The sample synthesized at pH = 8 with a lower surface area (10 m^2/g) and bismuth excess on the surface led to slightly lower acrolein selectivity at 360 °C (Figure 3b). Propylene conversion of the bismuth molybdates prepared at pH = 1 and pH = 9 did not exceed 6% at this temperature. The catalyst synthesized at pH = 9 with Bi/Mo = 2/3 composed of γ-Bi_2MoO_6 gave similar activity and selectivity as Bi1Mo1_pH9 at 320 °C and 360 °C (see Figure 3; $X_{propylene}$ < 5% and $X_{propylene}$ < 10%, respectively) in the oxidation of propylene to acrolein. Both samples synthesized at pH = 9 exhibited lower catalytic performance than the sample prepared by conventional co-precipitation CP_Bi2Mo1_450 consisting also of γ-Bi_2MoO_6 with a surface area of 6 m^2/g (this sample has been further characterized in Reference [50]). Bi2Mo3_pH4 showed a phase composition similar to Bi1Mo1_pH5 but with an additional nitrate phase and lower surface area (*cf.* Table 1) resulting in lower catalytic performance at 320 °C and 360 °C than the sample synthesized at pH = 4 with Bi/Mo = 1/1 (Figure 3). In general, the samples synthesized at pH = 4–8 with an initial Bi/Mo ratio of 1/1 yielded relatively high propylene conversion, along with a high selectivity for acrolein compared to the co-precipitated sample using Bi/Mo = 2/1 (compare Figure 3a,b with Figure 5).

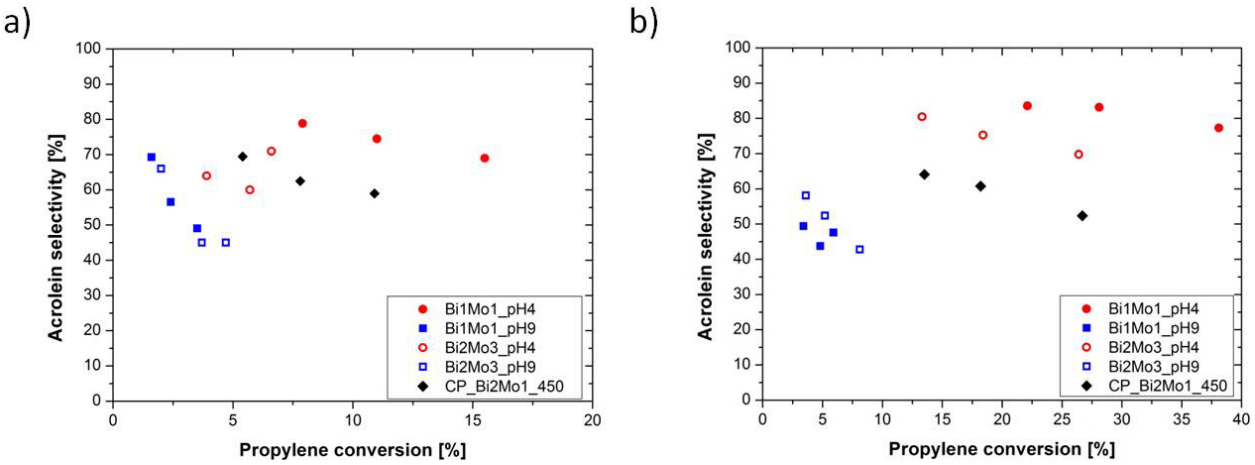

Figure 5. Comparison of the catalytic performance of the samples prepared at pH = 4 and pH = 9 with Bi/Mo = 1/1 and 2/3 and a reference sample synthesized by co-precipitation with Bi/Mo = 2/1 at 320 °C (**a**) and 360 °C (**b**). Reaction conditions: 500 mg catalyst; $C_3H_6/O_2/N_2$ = 5/25/70; 50, 80 and 120 NmL/min.

Bi1Mo1_pH9 showed low propylene conversion also at 400 °C (5%–9%) with acrolein selectivity below 50% and CO_2 selectivity of around 50% (Figure 3c), whereas the catalytic performance of the sample synthesized at pH = 1 increased strongly to propylene conversions of 22%–35% and acrolein selectivities of 74%–79%. For all the other samples the catalytic performance in propylene oxidation was only slightly increased when the temperature changed from 360 °C to 400 °C. The three samples synthesized at pH = 6–8 still exhibited the highest propylene conversion (35%–58%) of the tested samples with acrolein selectivities up to 92%. The sample synthesized at pH = 8, which was slightly less selective at 360 °C, gave the same acrolein selectivity as the samples synthesized at pH = 6–7 at 400 °C (Figure 3c). Further increase of the process temperatures to more than 400 °C did not result in an improvement of the catalytic activity. The corresponding full data set of propylene conversion and acrolein selectivities between 320 °C to 520 °C for the samples synthesized at pH = 5 (highest surface area) and pH = 6 (highest activity) as representative examples are given in the Supporting Information (Figure S4). An increase in temperature from 320 °C to 400 °C resulted in a better catalytic performance, whereas the activity at 440 °C was very similar to the one at 400 °C. At temperatures higher than 440 °C, the catalytic activity started to decrease and at 520 °C propylene conversion was similar to the values at 320 °C but with higher acrolein selectivities. The decrease in activity at temperatures higher than 440 °C was probably caused by a decrease in surface area for all samples. After application in propylene oxidation at 320 °C–520 °C the surface area of all used samples was ≤1 m^2/g, whereas after 8 h of calcination at 360 °C the samples synthesized at pH = 5 and pH = 6 still exhibited surface areas of 15 m^2/g and 16 m^2/g, respectively. The decrease in surface area already started at 360 °C, but the decrease was more significant between 400 °C and 440 °C when catalyst deactivation started.

Figure 6 shows the X-ray diffraction patterns of the samples after their application in the selective oxidation of propylene at 320 °C–520 °C. The phase composition of the samples synthesized at pH = 6–9 (γ-Bi_2MoO_6) did not change during the catalytic activity tests, but the hydrothermally prepared materials synthesized at pH = 1–5 were all composed of a mixture of α-$Bi_2Mo_3O_{12}$ and γ-Bi_2MoO_6 after use. This indicates that the reduced surface area, and not the phase transformation, was

the reason for the decreasing propylene conversion at temperatures above 440 °C. As already concluded earlier, a combination of the desired phase and a high surface area seemed to be crucial for propylene oxidation.

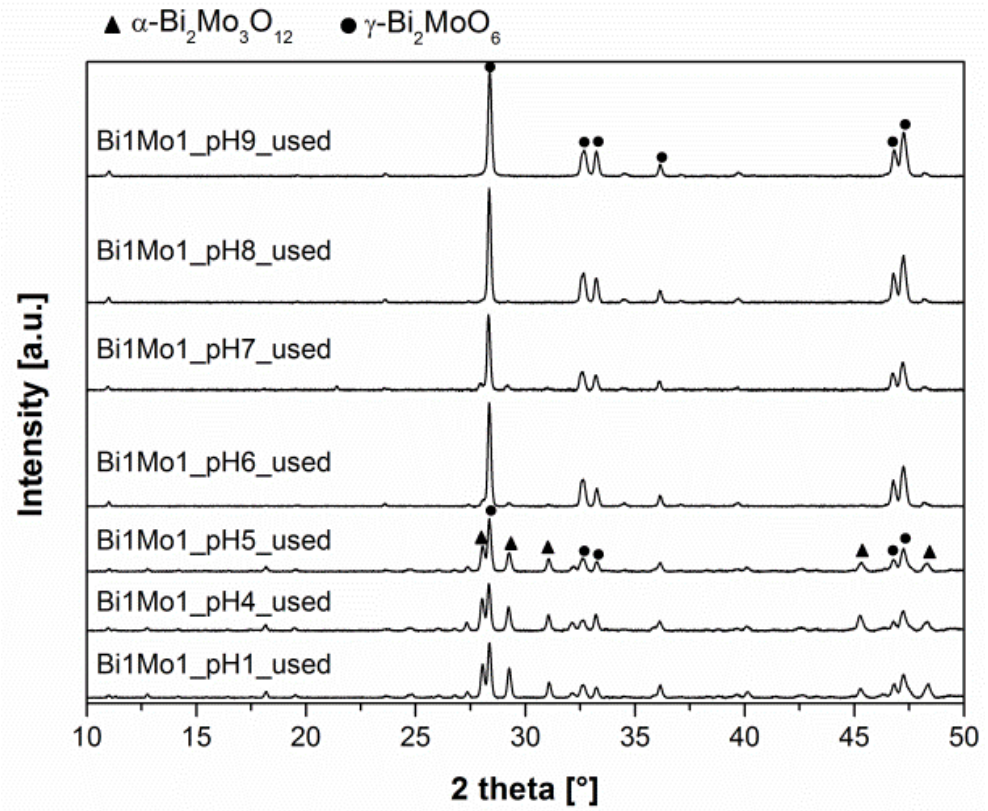

Figure 6. XRD patterns of the samples synthesized with Bi/Mo = 1/1 at different pH values after application in catalytic oxidation of propylene at temperatures up to 520 °C. The following symbols are used for marking the reflections of the different phases: α-$Bi_2Mo_3O_{12}$ (▲) and γ-Bi_2MoO_6 (●).

Jung *et al.* [60] tested the influence of the pH value during co-precipitation of γ-Bi_2MoO_6 (initial ratio Bi/Mo = 2/1) on the oxidative dehydrogenation of n-butylene and discovered that the sample synthesized at pH = 3 showed both the highest butylene conversion and 1,3-butadiene yield due to a high oxygen mobility of this sample. According to the group of Keulks [8,20], re-oxidation of the catalyst is the rate-determining step in propylene oxidation at temperatures below 400 °C, whereas abstraction of an α-hydrogen atom to form an allylic intermediate is the rate determining step at higher temperatures (>400 °C), in agreement with theory [14]. Recently, it was further reported that the reaction order in oxygen was zero at 340 °C and 400 °C for $Bi_2Mo_3O_{12}$ catalysts, *i.e.*, the reaction rate for acrolein formation, was independent of the partial pressure of oxygen, indicating that the transition temperature where re-oxidation of the catalyst becomes the rate determining step was lower than 340 °C [61,62]. The hydrothermally synthesized samples at pH = 4–8 exhibited high propylene conversion and also relatively high acrolein selectivities already at 360 °C. Therefore, oxygen mobility is not considered to be the decisive factor for the varying catalytic performance of the different samples depicted in Figure 3. The oxygen concentration used for the catalytic activity tests in this study was relatively high (C_3H_6/O_2 = 1/5) to

guarantee a complete re-oxidation of the bismuth molybdate catalysts and to minimize the effect of decreasing oxygen partial pressure if the reaction order was not zero.

Aleshina *et al.* [42] prepared bismuth molybdates by co-precipitation with a Bi/Mo ratio of 2 at pH values between 0 and 7 and with surface areas of 1–3 m^2/g and tested them in propylene oxidation in the presence of steam. They detected Bi_2O_3 in the sample prepared at pH = 7 and claimed that with increasing pH value molybdenum dissolved and remained in solution leading to a bismuth rich product (mixture of Bi_2O_3 and γ-Bi_2MoO_6), which showed lower propylene conversion (73% compared to 86%) and very low acrolein selectivity compared to the sample containing only γ-Bi_2MoO_6. In contrast, Bi_2O_3 was not detected in the present work. The samples synthesized at pH = 8 and 9 contained mainly γ-Bi_2MoO_6 and also the formation of hexadiene during propylene conversion was hardly observed, although, in the literature, it was reported that hexadiene was formed in the presence of Bi_2O_3 [63,64]. Thus, the reason for the low activity of Bi1Mo1_pH9 and the lower selectivity of Bi1Mo1_pH8 may not be contamination of the product with bismuth oxide but, rather, the lower surface areas compared to the samples synthesized at pH = 6 and 7.

3. Experimental Section

3.1. Catalyst Preparation

The bismuth molybdate materials were synthesized by hydrothermal synthesis similar to the procedure reported by Li *et al.* [36]. All chemicals were analytical grade and used without further purification.

In a typical synthesis, 10 mmol $Bi(NO_3)_3{\cdot}5H_2O$ and stoichiometric amounts of $(NH_4)_6Mo_7O_{24}{\cdot}4H_2O$ were dissolved in 20 mL 2.0 M nitric acid solution and 20 mL deionized water, respectively (for Bi/Mo = 1/1). The two solutions were mixed under vigorous stirring and the pH of the resulting mixture was adjusted to the desired value with an aqueous solution of 25 vol. % ammonia. For all samples addition of ammonia solution was necessary due to the low initial pH value. After stirring for 30 min the resulting solutions were heated to 180 °C in sealed 250 mL autoclaves (Berghof, Eningen, Germany) with Teflon inlays and kept in an oven for 24 h. Next, the solid product was separated by filtration at room temperature, and washed with 100 mL deionized water, 40 mL ethanol and finally 40 mL acetone. The resulting powder was dried at room temperature and ambient pressure. The samples are denoted as Bi*x*Mo*y*_pH with Bi/Mo = *x*/*y*.

For comparison co-precipitation was used to synthesize a reference sample with Bi/Mo = 2/1 according to Carrazán *et al.* [65] using $(NH_4)_6Mo_7O_{24}{\cdot}4H_2O$ dissolved in NH_4OH and $Bi(NO_3)_3{\cdot}5H_2O$ dissolved in HNO_3 at pH = 7. The resulting solid material was calcined at 450 °C to yield the γ-phase, and was referred to as CP_Bi2Mo1_450. This sample has been further studied and characterized in Reference [50].

3.2. Catalyst Characterization

X-ray diffraction (XRD) measurements were recorded using a Bruker D8 Advance powder diffractometer (Karlsruhe, Germany) in the range 2θ = 8°–80° (step size 0.016°) with Cu K_α radiation (Ni filter, 45 mA, 35 kV) on rotating sample holders. Raman spectra were recorded with a Horiba Jobin

Yvon spectrometer (LabRam, Palaiseau, France) attached to an Olympus microscope (BX 40, Hamburg, Germany) using a 632.8 nm laser in the range 100–1100 cm^{-1} without pre-treatment of the sample on an object slide.

The specific surface area (SSA) was measured by nitrogen adsorption at its boiling point (Belsorp II mini, BEL Japan Inc., Osaka, Japan) using multipoint BET theory in the p/p_0 = 0.05–0.3 range.

Surface analysis by X-ray photoelectron spectroscopy (XPS) was performed with a K-Alpha spectrometer (ThermoFisher Scientific, Braunschweig, Germany) using a micro focused Al K_α X-ray source (400 μm spot size). Data acquisition and processing using Thermo Avantage software (Braunschweig, Germany) is described elsewhere [66]. Charge compensation during analysis was achieved using electrons of 8 eV energy and low energy argon ions to prevent any localized charging. Spectra were fitted with one or more Voigt profiles (binding energy uncertainty: ±0.2 eV) [12,67]. Scofield sensitivity factors were applied for quantification [68]. Charging was corrected by shifting to the binding energy of C 1s (C–C, C–H) at 285.0 eV. The energy scale was calibrated by means of the well-known photoelectron peaks of metallic Cu, Ag and Au.

The bulk composition of the catalysts was determined by optical emission spectrometry with inductively coupled plasma (ICP-OES, Agilent 720/725-ES, Waldbronn, Germany). The plasma was created by a 40 MHz high-frequency generator and argon was applied as the plasma gas. For ICP-OES each sample was dissolved in 6 mL concentrated HNO_3, 2 mL concentrated HCl and 0.5 mL H_2O_2 in a microwave (at 600 W for 45 min).

X-ray absorption spectroscopy (XAS) was performed at beamline BM01B at the European Synchrotron Radiation Facility (ESRF, Grenoble, France). The samples were diluted with boron nitride and pressed to pellets for *ex situ* measurement in transmission mode at the Mo K edge (20.0 keV). XAS data were processed using the IFFEFIT software package (Chicago, IL, USA) [69].

3.3. Catalytic Tests

The catalytic performance was tested in a continuous flow fixed bed reactor, a U-shaped quartz reactor with 4 mm inner diameter. The catalyst powders were pressed into pellets, crushed and sieved to 150–300 μm particles, and 500 mg of sample were loaded in the reactor and stabilized with quartz wool. The quartz reactor was connected to a commercial test unit (ChimneyLab Europe, Hadsten, Denmark) with calibrated mass flow controllers (Brooks, Hatfield, PA, USA) and placed in an oven (Watlow, St. Louis, MO, USA) [70]. A thermocouple was placed inside the reactor just touching the catalyst bed to measure the reaction temperature and a pressure transducer placed upstream of the reactor measured the actual reaction pressure. The catalysts were pre-oxidized in dry air at 300 °C and activity tests were performed using a gas composition of $C_3H_6/O_2/N_2$ = 5/25/70 and flows of 50, 80, 120 NmL/min. The gas analysis was performed with a dual channel GC-MS (Thermo Fischer, Brauschweig, Germany) with a TCD detector for quantifying N_2, O_2, CO and CO_2 and a FID detector parallel to the MS for identification and quantification of saturated and unsaturated light hydrocarbons and oxygenated by-products. Before calculating the conversion of propylene and the selectivity for acrolein, the measured concentrations were corrected for expansion of the gas due to combustion using the nitrogen signal as internal standard.

4. Conclusions

In the present study different bismuth molybdate catalysts were synthesized using hydrothermal synthesis. The applied Bi/Mo ratio and the pH value had a strong influence on crystalline phases, specific surface area, bulk and surface composition and, thus, the catalytic performance. With increasing pH values from 1 to 9, the amount of more active γ-Bi_2MoO_6 compared to α-$Bi_2Mo_3O_{12}$ increased resulting in a higher catalytic activity.

The samples synthesized at pH = 4–7 exhibited relatively large surface areas (>20 m^2/g) compared to unsupported bismuth molybdates reported in literature. The higher surface area was beneficial for the catalytic activity in the selective oxidation of propylene under the applied conditions. The bismuth molybdates synthesized at pH = 6–7, which contained only γ-Bi_2MoO_6 and which exhibited high specific surface areas, yielded the highest propylene conversion at high acrolein selectivities. They were more active than samples with higher surface areas prepared at pH = 5, which also contained impurities of other phases. Very high (pH ≥ 9) or low (pH ≤ 1) pH values during synthesis led to catalysts with low catalytic activity and low specific surface area. This demonstrated that surface area is an important, but not the only, factor influencing activity, in agreement with literature.

Increasing the process temperature from 320 °C to 400 °C resulted in higher propylene conversion, while the catalysts deactivated at temperatures above 440 °C probably due to sintering and decreased specific surface area. Hence, especially at higher operating temperatures, stabilization of the surface area remains a key issue. Incorporation of further elements like Co, Fe or V, which are also included in industrial multicomponent bismuth molybdates, via hydrothermal synthesis could be beneficial for the stability of the prepared catalysts, as well as for the overall catalytic performance.

Acknowledgments

We thank the Danish Council for Strategic Research for financial support in the framework of the DSF proposal “Nanoparticle synthesis for catalysis” (grant No. 2106-08-0039). We gratefully acknowledge Hermann Köhler at the Institute of Catalysis Research and Technology (IKFT-KIT) for performing ICP-OES measurements and Angela Beilmann at Institute for Chemical Technology and Polymer Chemistry (ITCP-KIT) for the nitrogen physisorption measurements. The European Synchrotron Radiation Facility (ESRF) in Grenoble is acknowledged for providing XAS beamtime at the beamline BM01B. We thank Dmitry Doronkin and Hudson Carvalho (KIT) for the XAS measurements and Wouter van Beek (ESRF) for help and support during the beamtime.

Author Contributions

The experimental work and drafting of the manuscript was carried out by K.S., assisted by M.H. who performed catalytic measurements. V.T. and P.B. supported XPS and Raman experiments. W.K. participated in the interpretation of the scientific results and the preparation of the manuscript. J.-D.G. and A.D.J. supported the work and cooperation between DTU and KIT, supervised the experimental work, commented and approved the manuscript. The manuscript was written through comments and contributions of all authors. All authors have given approval to the final version of the manuscript.

Conflicts of Interest

The authors declare no conflict of interest.

References

1. Idol, J.D. Process for the Manufacture of Acrylonitrile. U.S. Patent 2,904,580, 15 September 1959.
2. Callahan, J.L.; Foreman, R.W.; Veatch, F. Attrition Resistant Oxidation Catalysts. U.S. Patent 3,044,966, 17 July 1962.
3. Grasselli, R.K.; Burrington, J.D. Selective oxidation and ammoxidation of propylene by heterogeneous catalysis. *Adv. Catal.* **1981**, *30*, 133–163.
4. Snyder, T.P.; Hill, C.G. The mechanism of the partial oxidation of propylene over bismuth molybdate catalysts. *Catal. Rev. Sci. Eng.* **1989**, *31*, 43–95.
5. Hoefs, E.V.; Monnier, J.R.; Keulks, G.W. Investigation of the type of active oxygen for the oxidation of propylene over bismuth molybdate catalysts using Infrared and Raman spectroscopy. *J. Catal.* **1979**, *57*, 331–337.
6. Batist, P.A. Bismuth molybdates—Preparation and catalysis. *J. Chem. Technol. Biotechnol.* **1979**, *29*, 451–466.
7. German, K.; Grzybows. B; Haber, J. Active centers for oxidation of propylene on Bi–Mo–O catalysts. *Acad. Pol. Sci. Chim.* **1973**, *21*, 319–325.
8. Krenzke, L.D.; Keulks, G.W. Catalytic oxidation of propylene 6. Mechanistic studies utilizing isotopic tracers. *J. Catal.* **1980**, *61*, 316–325.
9. Carson, D.; Coudurier, G.; Forissier, M.; Védrine, J.C.; Laarif, A.; Theobald, F. Synergy effects in the catalytic properties of bismuth molybdates. *J. Chem. Soc. Faraday Trans. 1* **1983**, *79*, 1921–1929.
10. Zhou, B.; Sun, P.; Sheng, S.; Guo, X. Cooperation between the α and γ phases of bismuth molybdate in the selective oxidation of propene. *J. Chem. Soc. Faraday Trans.* **1990**, *86*, 3145–3150.
11. Le, M.T.; van Well, W.J.M.; Stoltze, P.; van Driessche, I.; Hoste, S. Synergy effects between bismuth molybdate catalyst phases (Bi/Mo from 0.57 to 2) for the selective oxidation of propylene to arcrolein. *Appl. Catal. A* **2005**, *282*, 189–194.
12. Ayame, A.; Uchida, K.; Iwataya, M.; Miyamoto, M. X-ray photoelectron spectroscopic study on α- and γ-bismuth molybdate surfaces exposed to hydrogen, propene and oxygen. *Appl. Catal. A* **2002**, *227*, 7–17.
13. Hanna, T.A. The role of bismuth in the SOHIO process. *Coord. Chem. Rev.* **2004**, *248*, 429–440.
14. Getsoian, A.B.; Shapovalov, V.; Bell, A.T. DFT+U Investigation of Propene Oxidation over Bismuth Molybdate: Active Sites, Reaction Intermediates, and the Role of Bismuth. *J. Phys. Chem. C* **2013**, *117*, 7123–7137.
15. Morooka, Y.; Ueda, W. Multicomponent bismuth molybdate catalyst: A highly functionalized catalyst system for the selective oxidation of olefin. *Adv. Catal.* **1994**, *40*, 233–273.
16. Ueda, W.; Morooka, Y.; Ikawa, T.; Matsuura, I. Promotion effect of iron for the multicomponent bismuth molybdate catalysts as revealed by $^{18}O_2$ tracer. *Chem. Lett.* **1982**, 1365–1368.

17. Millet, J.M.M.; Ponceblanc, H.; Coudurier, G.; Herrmann, J.M.; Védrine, J.C. Study of multiphasic molybdate-based catalysts. 2. Synergy effect between bismuth molybdates and mixed iron cobalt molybdates in mild oxidation of propene. *J. Catal.* **1993**, *142*, 381–391.
18. Carson, D.; Forissièr, M.; Védrine, J.C. Kinetic study of the partial oxidation of propene and 2-methylpropene on different bismuth molybdate and on a bismuth iron molybdate phase. *J. Chem. Soc. Faraday Trans. 1* **1984**, *80*, 1017–1028.
19. Krenzke, L.D.; Keulks, G.W. The catalytic oxidation of propylene. 8. An investigation of kinetics over $Bi_2Mo_3O_{12}$, Bi_2MoO_6 and $Bi_3FeMo_2O_{12}$. *J. Catal.* **1980**, *64*, 295–302.
20. Monnier, J.R.; Keulks, G.W. The catalytic oxidation of propylene. 9. The kinetics and mechanism over β-$Bi_2Mo_2O_9$. *J. Catal.* **1981**, *68*, 51–66.
21. Brazdil, J.F.; Suresh, D.D.; Grasselli, R.K. Redox kinetics of bismuth molybdate ammoxidation catalysts. *J. Catal.* **1980**, *66*, 347–367.
22. Schuh, K.; Kleist, W.; Høj, M.; Trouillet, V.; Jensen, A.D.; Grunwaldt, J.-D. One-step synthesis of bismuth molybdate catalysts via flame spray pyrolysis for the selective oxidation of propylene to acrolein. *Chem. Commun.* **2014**, *50*, 15404–15406.
23. Snyder, T.P.; Hill, C.G. Stability of bismuth molybdate catalysts at elevated temperatures in air under reaction conditions. *J. Catal.* **1991**, *132*, 536–555.
24. Batist, P.A.; Bouwens, J.F.H.; Schuit, G.C.A. Bismuth molybdate catalysts—Preparation, characterization and activity of different compounds in Bi–Mo–O System. *J. Catal.* **1972**, *25*, 1–11.
25. Keulks, G.W.; Hall, J.L.; Daniel, C.; Suzuki, K. Catalytic oxidation of propylene. 4. Preparation and characterization of α-bismuth molybdate. *J. Catal.* **1974**, *34*, 79–97.
26. Soares, A.P.V.; Dimitrov, L.D.; de Oliveira, M.; Hilaire, L.; Portela, M.F.; Grasselli, R.K. Synergy effects between beta and gamma phases of bismuth molybdates in the selective catalytic oxidation of 1-butene. *Appl. Catal. A* **2003**, *253*, 191–200.
27. Rastogi, R.P.; Singh, A.K.; Shukla, C.S. Kinetics and mechanism of solid-state reaction between bismuth(III) oxide and molybdenum(VI) oxide. *J. Solid State Chem.* **1982**, *42*, 136–148.
28. Thang, L.M.; Bac, L.H.; van Driessche, I.; Hoste, S.; van Well, W.J.M. The synergy effect between gamma and beta phase of bismuth molybdate catalysts: Is there any relation between conductivity and catalytic activity? *Catal. Today* **2008**, *131*, 566–571.
29. Le, M.T.; van Craenenbroeck, J.; van Driessche, I.; Hoste, S. Bismuth molybdate catalysts synthesized using spray drying for the selective oxidation of propylene. *Appl. Catal. A* **2003**, *249*, 355–364.
30. Van Well, W.J.M.; Le, M.T.; Schiødt, N.C.; Hoste, S.; Stoltze, P. The influence of the calcination conditions on the catalytic activity of Bi_2MoO_6 in the selective oxidation of propylene to acrolein. *J. Mol. Catal. A* **2006**, *256*, 1–8.
31. Nell, A.; Getsoian, A.B.; Werner, S.; Kiwi-Minsker, L.; Bell, A.T. Preparation and Characterization of High-Surface-Area $Bi_{(1-x)/3}V_{1-x}Mo_xO_4$ Catalysts. *Langmuir* **2014**, *30*, 873–880.
32. Shi, Y.; Feng, S.; Cao, C. Hydrothermal synthesis and characterization of Bi_2MoO_6 and Bi_2WO_6. *Mater. Lett.* **2000**, *44*, 215–218.
33. Beale, A.M.; Sankar, G. *In situ* study of the formation of crystalline bismuth molybdate materials under hydrothermal conditions. *Chem. Mater.* **2003**, *15*, 146–153.

34. Yu, J.Q.; Kudo, A. Hydrothermal synthesis and photocatalytic property of 2-dimensional bismuth molybdate nanoplates. *Chem. Lett.* **2005**, *34*, 1528–1529.
35. Xie, H.; Shen, D.; Wang, X.; Shen, G. Microwave hydrothermal synthesis and visible-light photocatalytic activity of γ-Bi_2MoO_6 nanoplates. *Mater. Chem. Phys.* **2008**, *110*, 332–336.
36. Li, H.; Li, K.; Wang, H. Hydrothermal synthesis and photocatalytic properties of bismuth molybdate materials. *Mater. Chem. Phys.* **2009**, *116*, 134–142.
37. Gruar, R.; Tighe, C.J.; Reilly, L.M.; Sankar, G.; Darr, J.A. Tunable and rapid crystallisation of phase pure Bi_2MoO_6 (koechlinite) and $Bi_2Mo_3O_{12}$ via continuous hydrothermal synthesis. *Solid State Sci.* **2010**, *12*, 1683–1686.
38. Kongmark, C.; Coulter, R.; Cristol, S.; Rubbens, A.; Pirovano, C.; Loefberg, A.; Sankar, G.; van Beek, W.; Bordes-Richard, E.; Vannier, R.-N. A Comprehensive Scenario of the Crystal Growth of γ-Bi_2MoO_6 Catalyst during Hydrothermal Synthesis. *Cryst. Growth Des.* **2012**, *12*, 5994–6003.
39. Yoshimura, M.; Byrappa, K. Hydrothermal processing of materials: Past, present and future. *J. Mater. Sci.* **2008**, *43*, 2085–2103.
40. Zhang, L.; Xu, T.; Zhao, X.; Zhu, Y. Controllable synthesis of Bi_2MoO_6 and effect of morphology and variation in local structure on photocatalytic activities. *Appl. Catal. B* **2010**, *98*, 138–146.
41. Ren, J.; Wang, W.; Shang, M.; Sun, S.; Gao, E. Heterostructured Bismuth Molybdate Composite: Preparation and Improved Photocatalytic Activity under Visible-Light Irradiation. *ACS Appl. Mater. Interfaces* **2011**, *3*, 2529–2533.
42. Aleshina, G.I.; Joshi, C.; Tarasova, D.V.; Kustova, G.N.; Nikoro, T.A. Catalytic properties of Bi/Mo oxide catalysts prepared via precipitation. *React. Kinet. Catal. Lett.* **1984**, *26*, 203–208.
43. Guo, C.; Xu, J.; Wang, S.; Li, L.; Zhang, Y.; Li, X. Facile synthesis and photocatalytic application of hierarchical mesoporous Bi_2MoO_6 nanosheet-based microspheres. *Cryst. Eng. Commun.* **2012**, *14*, 3602–3608.
44. Beale, A.M.; Jacques, S.D.M.; Sacaliuc-Parvalescu, E.; O'Brien, M.G.; Barnes, P.; Weckhuysen, B.M. An iron molybdate catalyst for methanol to formaldehyde conversion prepared by a hydrothermal method and its characterization. *Appl. Catal. A* **2009**, *363*, 143–152.
45. Zhang, L.; Zhang, Y.; Dai, H.; Deng, J.; Wei, L.; He, H. Hydrothermal synthesis and catalytic performance of single-crystalline $La_{2-x}Sr_xCuO_4$ for methane oxidation. *Catal. Today* **2010**, *153*, 143–149.
46. Salamanca, M.; Licea, Y.E.; Echavarria, A.; Faro, A.C., Jr.; Palacio, L.A. Hydrothermal synthesis of new wolframite type trimetallic materials and their use in oxidative dehydrogenation of propane. *Phys. Chem. Chem. Phys.* **2009**, *11*, 9583–9591.
47. Ueda, W.; Oshihara, K. Selective oxidation of light alkanes over hydrothermally synthesized Mo–V–M–O (M = Al, Ga, Bi, Sb, and Te) oxide catalysts. *Appl. Catal. A* **2000**, *200*, 135–143.
48. Botella, P.; Garcia-Gonzalez, E.; Dejoz, A.; Nieto, J.M.L.; Vazquez, M.I.; Gonzalez-Calbet, J. Selective oxidative dehydrogenation of ethane on MoVTeNbO mixed metal oxide catalysts. *J. Catal.* **2004**, *225*, 428–438.

49. Sanfiz, A.C.; Hansen, T.W.; Girgsdies, F.; Timpe, O.; Rödel, E.; Ressler, T.; Trunschke, A.; Schlögl, R. Preparation of Phase-Pure M1 MoVTeNb Oxide Catalysts by Hydrothermal Synthesis—Influence of Reaction Parameters on Structure and Morphology. *Top. Catal.* **2008**, *50*, 19–32.
50. Schuh, K.; Kleist, W.; Høj, M.; Trouillet, V.; Beato, P.; Jensen, A.D.; Patzke, G.R.; Grunwaldt, J.-D. Selective oxidation of propylene to acrolein by hydrothermally synthesized bismuth molybdates. *Appl. Catal. A* **2014**, *482*, 145–156.
51. Hardcastle, F.D.; Wachs, I.E. Molecular structure of molybdenum oxide in bismuth molybdates by Raman spectroscopy. *J. Phys. Chem.* **1991**, *95*, 10763–10772.
52. Noack, J.; Rosowski, F.; Schlögl, R.; Trunschke, A. Speciation of Molybdates under Hydrothermal Conditions. *Z. Anorg. Allg. Chem.* **2014**, *640*, 2730–2736.
53. Briand, G.G. Bifunctional Ligands in Discerning and Developing the Fundamental and Medicinal Chemistry of Bismuth(III). Ph.D. Thesis, Dalhousie University, Halifax, NS, Canada, July 1999.
54. Trifiro, F.; Scarle, R.D.; Hoser, H. Relationships between structure and activity of mixed oxides as oxidation catalyst. 1. Preparation and solid state reactions of Bi-molybdates. *J. Catal.* **1972**, *25*, 12–24.
55. Dewangan, K.; Sinha, N.N.; Sharma, P.K.; Pandey, A.C.; Munichandraiah, N.; Gajbhiye, N.S. Synthesis and characterization of single-crystalline α-MoO_3 nanofibers for enhanced Li-ion intercalation applications. *Cryst. Eng. Commun.* **2011**, *13*, 927–933.
56. Chen, L.; Aarcon-Lado, E.; Hettick, M.; Sharp, I.D.; Lin, Y.; Javey, A.; Ager, J.W. Reactive Sputtering of Bismuth Vanadate Photoanodes for Solar Water Splitting. *J. Phys. Chem. C* **2013**, *117*, 21635–21642.
57. Choi, J.G.; Thompson, L.T. XPS study of as-prepared and reduced molybdenum oxides. *Appl. Surf. Sci.* **1996**, *93*, 143–149.
58. Herrmann, J.M.; el Jamal, M.; Forissier, M. Evidence by electrical conductivity for an excess of bismuth as Bi^+ interstitial at the surface of gamma-phase Bi_2MoO_6—Consequence for selectivity in propene catalytic oxidation. *React. Kinet. Catal. Lett.* **1988**, *37*, 255–260.
59. Ruckenstein, E.; Krishnan, R.; Rai, K.N. Oxygen depletion of oxide catalysts. *J. Catal.* **1976**, *45*, 270–273.
60. Jung, J.C.; Kini, H.; Choi, A.S.; Chung, Y.-M.; Kim, T.J.; Lee, S.J.; Oh, S.-H.; Song, I.K. Effect of pH in the preparation of γ-Bi_2MoO_6 for oxidative dehydrogenation of *n*-butene to 1,3-butadiene: Correlation between catalytic performance and oxygen mobility of γ-Bi_2MoO_6. *Catal. Commun.* **2007**, *8*, 625–628.
61. Zhai, Z.; Getsoian, A.B.; Bell, A.T. The kinetics of selective oxidation of propene on bismuth vanadium molybdenum oxide catalysts. *J. Catal.* **2013**, *308*, 25–36.
62. Zhai, Z.; Wang, X.; Licht, R.; Bell, A.T. Selective oxidation and oxidative dehydrogenation of hydrocarbons on bismuth vanadium molybdenum oxide. *J. Catal.* **2015**, *325*, 87–100.
63. Grzybowska, B.; Haber, J.; Janas, J. Interaction of allyl iodide with molybdate catalysts for selective oxidation of hydrocarbons. *J. Catal.* **1977**, *49*, 150–163.
64. Swift, H.E.; Bozik, J.E.; Ondrey, J.A. Dehydrodimerization of propylene using bismuth oxide as oxidant. *J. Catal.* **1971**, *21*, 212–224.

65. Carrazán, S.R.G.; Martin, C.; Rives, V.; Vidal, R. Selective oxidation of isobutene to methacrolein on multiphasic molybdate-based catalysts. *Appl. Catal. A* **1996**, *135*, 95–123.
66. Parry, K.L.; Shard, A.G.; Short, R.D.; White, R.G.; Whittle, J.D.; Wright, A. ARXPS characterisation of plasma polymerised surface chemical gradients. *Surf. Interface Anal.* **2006**, *38*, 1497–1504.
67. Grunwaldt, J.-D.; Wildberger, M.D.; Mallat, T.; Baiker, A. Unusual redox properties of bismuth in sol-gel Bi–Mo–Ti mixed oxides. *J. Catal.* **1998**, *177*, 53–59.
68. Scofield, J.H. Hartree-Slater subshell photoionization cross-sections at 1254 and 1487eV. *J. Electron Spectrosc. Relat. Phenom.* **1976**, *8*, 129–137.
69. Ravel, B.; Newville, M. ATHENA, ARTEMIS, HEPHAESTUS: Data analysis for X-ray absorption spectroscopy using IFEFFIT. *J. Synchrotron Radiat.* **2005**, *12*, 537–541.
70. Høj, M.; Jensen, A.D.; Grunwaldt, J.-D. Structure of alumina supported vanadia catalysts for oxidative dehydrogenation of propane prepared by flame spray pyrolysis. *Appl. Catal. A* **2013**, *451*, 207–215.